

# Morphological Evolution of Sub-nanometer SiC Surface Steps upon Graphitization via Electron Channeling Contrast Imaging

## Application Note

Nicola Ferralis, Jason Kawasaki, Carlo Carraro, Roya Maboudian  
Department of Chemical Engineering, University of California, Berkeley

Jim Rynne, James Spallas, Lawrence Muray  
Agilent Technologies

### Introduction

Graphene has been shown recently to possess many of the remarkable electronic properties of carbon nanotubes [1], while lending itself more readily to the planar paradigm of integrated-circuit fabrication processes [2, 3]. Epitaxial graphene (epigraphene) on silicon carbide (SiC) surfaces is emerging as an attractive process alternative to the painstaking layer-by-layer exfoliation of graphite crystals [4].

Epigraphene shares the key electron transport properties of freestanding exfoliated films [1–4]. However, in contrast to the exfoliated films, new features in the electronic [1, 5, 6] and surface structure [7–9] appear in epitaxial graphene grown on the (0001) surface of 6H-SiC. The novel electronic properties and the choice of the type of substrate are significant for the design of nonlinear devices and underscores the importance of substrate interactions in epitaxial films. The interaction of epigraphene with the SiC substrate is mediated by a monolayer of C atoms, a so-called “buffer layer,” arranged in a honeycomb lattice, like graphene, but

bonded in an  $sp^3$  configuration, with each atom forming a covalent bond to a Si atom beneath [4]. This buffer layer evolves from C-rich, high temperature surface reconstructions of 6H-SiC (0001) upon thermal desorption of Si atoms around  $T = 1100^\circ\text{C}$ . Annealing to higher temperature ( $1250^\circ\text{C}$ ) results in further desorption of Si, which promotes the formation of a second carbon layer, and deprives the original (topmost) carbon atoms of their covalent bonds to Si atoms, inducing the  $sp^2$  bonding configuration, i.e., into that of a graphene layer [2,10].

The highly disruptive nature of the process induces a substantial change in the surface morphology. For example, upon high temperature annealing needed to achieve optimal graphitization in a single crystalline SiC surface, the graphitization process induces a significant amount of step edge roughening [11]. This process is a consequence of the preferred graphitization at step edges. Therefore imaging at high resolution (both lateral and vertical) the evolution in the morphology of surface steps is crucial in order to understand the effects of different graphitization



Agilent Technologies

conditions. Often low-energy electron microscopy (LEEM) is employed for the purpose [11]. However the lateral resolution is confined to ~20 nm, despite its high vertical resolution (below 0.2 nm). Furthermore, the high cost of operation (which includes ultrahigh vacuum - UHV - conditions) limits the LEEM applicability in routine imaging of graphitized SiC for device applications. Alternatively, atomic force microscopy provide the required high lateral and vertical resolution [11, 12]. However the limitations on the sample size (die-level) reduce its application for non-invasive, non-destructive wafer-scale imaging.

Scanning electron microscopy (SEM) is commonly employed to measure morphological features in the plane of the sample since they provide high lateral resolution. Furthermore, SEM provides the ability to image wafer-scale samples non-destructively. Although quantitative information in the third dimension is not possible at the same resolution, the presence or absence of certain topographic features is often sufficient for many applications [13]. However, the high penetration depth (~100 nm) determined by the high primary voltage (>5 keV) limits the ability to resolve vertical features (such as surface steps) below few nanometers. In order to overcome these limitations, electron channeling contrast imaging (ECCI) was developed allowing the vertical resolution to be further improved resulting in the ability to image individual dislocations, atomic steps and other defects on or near the surface [13, 14]. While promising, however, the current implementation of ECCI-capable SEM still requires specialized electron detectors, and highly tilted samples (>70°). Additionally, at the high voltages

required for solid state detectors (typically >5 keV), only a small fraction of the total signal contains information about the surface.

In this application note, the Agilent 8500 FE-SEM, with the electron detector operating in differential or “topographic” mode (to remove the background signal and therefore to improve surface contrast) is employed in ECCI mode to measure the evolution of surface steps in polished and etched 6H-SiC wafers with sub-nm resolution [14]. Both backscattered and secondary electrons were collected to enhance the signal-to-noise ratio of the images. Even without specialized hardware, the sensitivity of the technique due to electron channeling was sufficiently high to clearly resolve sub-nm steps on the surface of the wafer. Simple data processing allowed the full characterization of evolution of step roughening depending on the graphitization conditions, also allowing a direct comparison of such evolution with other properties (such as surface strain in graphene) measured with complementary techniques (such as Raman spectroscopy [7-15]).

### Experimental Details

6H-SiC single crystal samples with (0001) orientation (CREE Research, Inc.) were first prepared ex vacuo by high temperature annealing (~1550 to 1700°C) in hydrogen atmosphere to obtain a regularly stepped surface, as described elsewhere [7]. The stepped surface is necessary to monitor the morphological evolution of epitaxial graphene as it grows off SiC terrace edges [11]. The resulting SiC surface was characterized by a sharp ( $3 \times 3$ ) low-energy electron diffraction

(LEED) pattern. Graphene epilayers were produced by additional thermal annealing the Si-face of 6H-SiC single crystals surfaces. Graphene layers were grown by annealing the SiC substrate in ultrahigh vacuum (UHV) for varied times (ranging from 1 to 30 minutes); subsequently, the substrate was cooled down to room temperature at the rate of  $\leq 1 \text{ Ks}^{-1}$ . The same growth temperature  $T_G = 1250 \pm 20^\circ \text{C}$  was used, in order to obtain the same number of graphene epilayers [4]. The film thickness was measured after the annealing by monitoring the C:Si Auger electron spectroscopy (AES) ratio [4]. In all data presented here on the graphitized substrate, the thickness of the graphene epilayer is  $1.0 \pm 0.2$  monolayer (ML).

Surface morphology was monitored by the Agilent 8500 FE-SEM which was used in a standard configuration, with working distance from 1 mm to 10 mm and with probe currents up to 2 nA. Under optimum conditions (namely, a 1.75 mm working distance and a 1 keV beam voltage) sub-10 nm lateral resolution is achieved. ECCI is achieved using a quad-segmented microchannel plate (MCP) detector assembly located directly below the objective lens. The detector collects backscattered electrons and, depending on the bias applied to the front plate, accepts or rejects secondary electrons. The MCP may be operated in either a standard mode, where all the channels are added together, or in a differential or topographic mode, in which opposite sides of the detector are dynamically subtracted. The effect is similar to repositioning a light source in optical microscopy at glancing incidence.

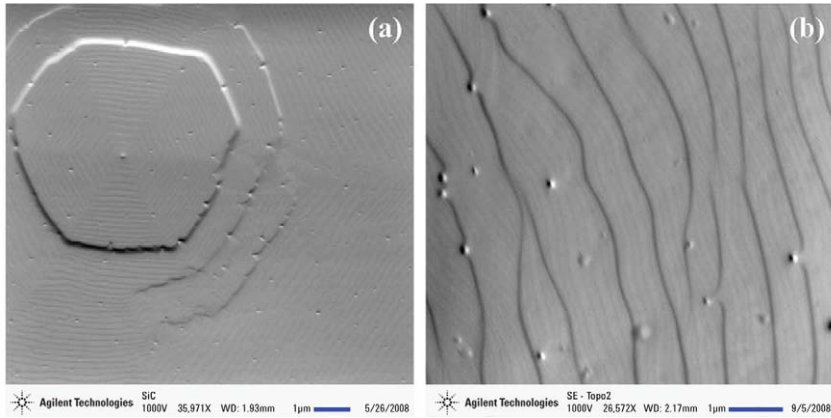


Figure 1. (a) Hillocks, terraces and defects on 6H-SiC sample. (b) The fine structure on the terraces was determined to be sub-nm atomic steps [13].

## Results and Discussion

### Sub-nm imaging of ungraphitized SiC surface steps

Representative micrographs of the ungraphitized SiC samples, imaged in topographic mode, are shown in Figure 1. Several surface features are evident, including, point defects and terraced planes. In Figure 1a, hexagonal structures that formed around a defect create hillocks with very high contrast edges. The terraced planes in Figure 1a are visible even with  $>0.1$  mm square field when viewing in topographic mode. Close examination of the terraces shown in Figure 1a reveals an additional fine structure evident in Figure 1b. In those areas of the wafer free from hillocks or other large defects, the pitch of the fine structure measured using a line scan through the image is found to be  $\sim 160$  nm. These fine features are visible in both backscatter and secondary+backscatter topographic modes but invisible in any of the non-topographic modes. To quantify the vertical size of these features, the sample was imaged using an atomic force microscope (AFM). The step height and pitch of the large

terraces average  $1.3 \mu\text{m}$  and  $28$  nm, respectively. An AFM image of just the fine structure is shown in Figure 2a. The measured pitch is  $\sim 170$  nm which was consistent with the values measured using the ECCI images. The measured step height is  $\sim 0.8$  nm, and thus confirming SEM imaging of sub-nm steps. As a crosscheck, the expected pitch of  $0.8$  nm steps can be calculated if the orientation of the silicon carbide is known. For these samples with  $\sim 0.4^\circ$  tilt off the  $[0\ 0\ 0\ 1]$  axis

(hexagonal crystal structure with lattice parameters  $a = 3 \text{ \AA}$  and  $c = 15 \text{ \AA}$ ), the calculated pitch is between  $100$  nm and  $200$  nm. With a separation between  $[0\ 0\ 0\ 1]$  planes of  $2.5 \text{ \AA}$ , a  $0.8$  nm step height represents three atomic planes [8-11], or half the repeating stack height of the 6H polytype at each terrace. Picard *et al.* observed similar results in 4H-SiC using ECCI and AFM [16].

Although many possible surface contrast mechanisms may be responsible for the sub-nm resolution, the electron channeling contrast imaging is the primary mechanism responsible for the enhanced contrast at atomic terrace edges. Edge effects, sample tilt angle, material contrast cannot account for the high vertical resolution, since the fine structure is only visible in topographic mode. The backscatter yield is directly related to the image contrast and is a function of the relative angle between a crystallographic plane and the incident primary beam (the Bloch wave). Therefore, if the beam is positioned at a fixed angle but scanned over an area, any change in crystal orientation or interlayer

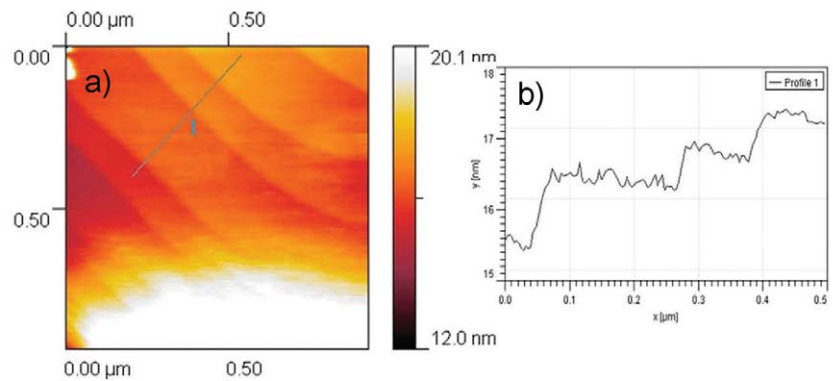


Figure 2. a) Atomic force micrograph of 6H-SiC sample on a terrace at roughly the same locations as shown in Figure 1b. b) line profile corresponding to the linescan "1" on the topographic image a). Steps are typically  $8 \text{ \AA}$  high, and they have a  $170$  nm pitch [13].

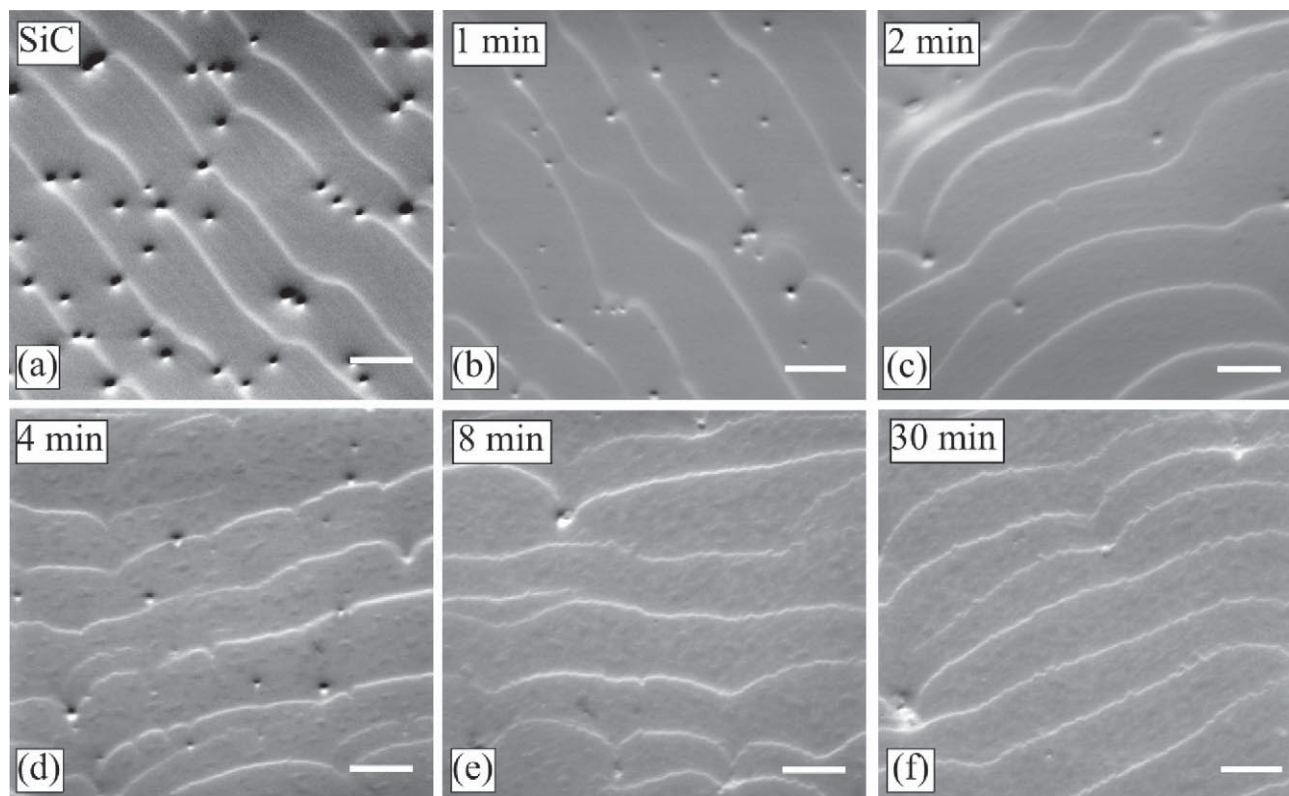


Figure 3. Electron channeling contrast images of 1 ML epitaxial graphene layers synthesized on SiC single crystal substrates at different annealing times: (a) clean SiC surface (0 min); (b) 1 min; (c) 2 min; (d) 4 min; (e) 8 min; (f) 30 min [8]. Scale bar: 1  $\mu\text{m}$ .

spacing results in a change in contrast. The most sensitive position and greatest change occurs when the beam is aligned exactly at the Bragg angle. A less sensitive and lower contrast mechanism occurs when elastic scattering events near the surface create a secondary divergent source of electrons (secondary Bloch waves) which, in turn, further modulate the backscatter yield. In TEM studies of atomic steps on Si(111), Pohl *et al.*, surmised that strain at the edges of steps produces a local change in the Bragg condition, thereby producing image contrast [17]. Similarly, as suggested by Trager-Cowan *et al.*, contrast change on the 6H-SiC samples could be interpreted as the displacement of the atoms at the step edge [18].

This suggests that backscatter yield changes at the edge of steps. In the differential topographic mode, the 8500 could detect these shifts and as a consequence produce channeling contrast.

#### **Morphological evolution of SiC surface steps upon graphitization.**

The ability to image three SiC bilayers is crucial for the characterization of the morphological evolution of the SiC surface upon graphitization, since the carbon density of three SiC bilayers is required to form a single layer of graphene. Therefore any change in morphology in the fine structures resolved can be directly associated with the formation of single layers of epitaxial graphene.

Figure 3(a) shows the images of the SiC surface after the high temperature annealing in hydrogen ambient, but before the high temperature graphitization in UHV. Two sets of terrace edges are visible: major step bunches spaced about 1.1  $\mu\text{m}$ , and subterraces spaced about 200 nm. As previously noted, terrace edges are 0.8 nm high, corresponding to three SiC bilayers. Terrace edges of the step bunches in the clean surface appear smooth and the subterraces can be clearly resolved. Electron channeling contrast images micrographs of a monolayer (ML) graphene grown in UHV for different annealing times at  $T_G = 1250^\circ\text{C}$  are shown in Figures 3(b)-(e). With increased annealing time, the major terrace edges become visibly rougher, while

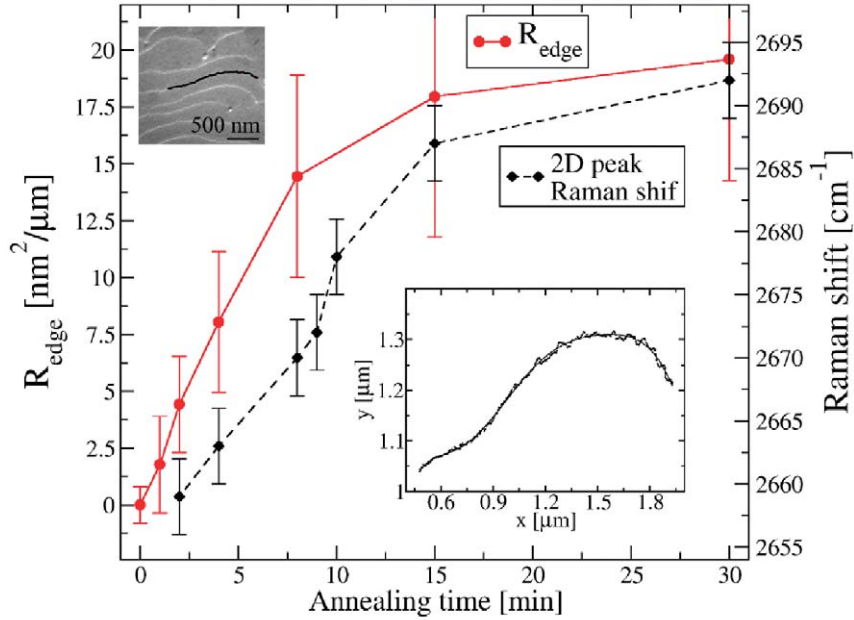


Figure 4. The edge roughness  $R_{\text{edge}}$  (defined in the main text) and the 2D Raman shift line [7] are shown as a function of annealing time. Several profiles of terrace edges are extracted from ECCI images of samples prepared with the same annealing time and temperature. Each profile (black curve on the ECCI image of a sample annealed for 8 minutes) is fit with a 9th order polynomial to obtain an edge baseline. The normalized average mean square deviation (and thus the edge roughness  $R_{\text{edge}}$ ) is extracted from the baseline [8].

the subterraces are much less clearly resolved. In order to quantify the extent of the roughening, the images were used to extract the mean square roughness of the step bunches as a function of annealing time. Plot digitizing software was used to trace several terrace edges at a sampling rate of about 17 nm/step (inset in Figure 4). A 9th order polynomial was used to fit the trace, which provides the baseline fit  $y_0(t)$ .

The average mean square (MS) deviation was extracted from the baseline  $y_0(t)$  and the trace. For each terrace edge, the average MS deviation was normalized by  $L$ , since the average MS deviation was found to be proportional to the edge length  $L$ . Finally, the difference in

the normalized MS deviation of any graphitized terrace edge with that of the initial ungraphitized surface was defined as  $R_{\text{edge}}$ . (Thus,  $R_{\text{edge}}$  for initial surface is zero). The evolution in  $R_{\text{edge}}$  with annealing time is shown in Figure 4. The sharp increase in step edge roughness occurs during the first 8-10 minutes of annealing, when  $R_{\text{edge}}$  rises to about  $15 \text{ nm}^2/\mu\text{m}$ . For longer annealing times, the edge roughness increases more gradually to a maximum of about  $20 \text{ nm}^2/\mu\text{m}$ . In addition to edge roughening, SiC subterraces become increasingly rougher and finally appear to aggregate into large patches (Figure 3(d)-(f)). This process develops until much of the higher SiC step edge is consumed to form a graphene layer on the lower terrace. The variation in

the terrace edge morphology observed here is related to the local dissolution of the SiC steps and the formation of graphene layers. However, such variation at constant growth temperature does not appear to alter the surface coverage considerably ( $\pm 0.2 \text{ ML}$ , based on AES).

The strain relaxation at  $T_G$ , implied by the Raman data [7], provides a likely explanation for the changes in morphology observed by ECCI. For long enough annealing times, the observed break up of the pinned graphene layer on the SiC subterraces into a patchy film relieves the tensile strain developed at  $T_G$ . These changes in morphology must be accompanied by roughening of the step edges to which graphene films are pinned.

Such increase in roughness does not induce a significant change in surface coverage ( $\pm 0.2$  ML). For shorter annealing times, SiC terraces are left morphologically unchanged, since surface relaxation does not take place.

### Conclusions

Using the Agilent 8500 FE-SEM for low-voltage electron channeling contrast imaging (LV-ECCI) at normal incidence, sub-nm steps on 6H-SiC were resolved. The particular geometry of the low-voltage scanning electron microscope system combined with a high brightness Schottky source and a four quadrant detector allowed imaging of steps, defects, voids and hillocks with no additional hardware. The LV-ECCI capability was used to image evolution in the surface morphology of epitaxial graphene films and of the underlying 6H-SiC

substrate. The observed behavior was explained in terms of the changes in structural strain during the synthesis of epitaxial graphene. It is found that long annealing times produce epitaxial graphene layers on SiC that are in equilibrium at growth temperature (and thus under highly compressive strain at room temperature); the development of large step roughness (as high as  $20 \text{ nm}^2/\mu\text{m}$ ) and film discontinuity develop as a consequence of stress relief at the growth temperature. Shorter annealing times result in highly tensile films at growth temperature, leading to almost stress-free films at room temperature as well as minimal change in surface morphology. Thus the ability to control strain in epitaxial graphene, by tuning of the annealing times, is tied with the ability to control the film morphology.

## References

- [1] K.S. Novoselov, A.G. Geim, S.V. Morozov, D. Jiang, Y. Zhang, S.V. Dubonos, I.V. Grigorieva, and A.A. Firsov, *Science* 306, 666 (2004).
- [2] F. Schwierz, *Nat. Nano.* 5, 487 (2010).
- [3] Y.-M. Lin, C. Dimitrakopoulos, K. Jenkins, D. Farmer, H.-Y. Chiu, A. Grill, and P. Avouris, *Science* 327, 662 (2010).
- [4] J. Hass, W. de Heer, and E. Conrad, *J. Phys: Condens Matter* 20, 323202 (2008).
- [5] S. Zhou, G.-H. Gweon, A. Fedorov, P. First, W. de Heer, D.-H. Lee, F. Guinea, A. Castro Neto, and A. Lanzara, *Nat. Mat.* 6, 770 (2007).
- [6] A. Bostwick, T. Ohta, T. Seyller, K. Horn, and E. Rotemberg, *Nat. Phys.* 3, 36 (2007).
- [7] N. Ferralis, R. Maboudian, and C. Carraro, *Phys. Rev. Lett.* 101, 156801 (2008).
- [8] N. Ferralis, J. Kawasaki, R. Maboudian, and C. Carraro, *Appl. Phys. Lett.* 93, 191916 (2008).
- [9] J. Roehrl, M. Hundhausen, K.V. Emtsev, Th. Seyller, R. Graupner, and L. Ley, *Appl. Phys. Lett.* 92, 201918 (2008).
- [10] I. Forbeaux, J.-M. Themlin, and J.-M. Debever, *Phys. Rev. B* 58, 16396 (1998) and references therein.
- [11] J. B. Hannon and R. M. Tromp, *Phys. Rev. B* 77, 241404 (2008).
- [12] T. Filleter, K. V. Emtsev, Th. Seyller, and R. Bennewitz, *Appl. Phys. Lett.* 93, 133117 (2008).
- [13] L. Muray, J. Spallas, C. Silver, S. Indermuehle, N. Ferralis, C. Carraro, R. Maboudian, *Microelectronic Engineering* 86, 1004–1008 (2009).
- [14] B.A. Simkin, M.A. Crimp, *Ultramicroscopy* 77 (1999) 65–75.
- [15] N. Ferralis, *J. Mat. Scie.* (2010) in press (doi: 10.1007/s10853-010-4673-3).
- [16] Y.N. Picard, M.E. Twigg, J.D. Caldwell, C.R. Eddy Jr., P.G. Neudeck, A.J. Trunek, *et al.*, *Appl. Phys. Lett.* 90 (2007) 234101.
- [17] O. Pohland, X. Tong, J.M. Gibson, *J. Vac. Sci. Technol. A* 11 (3) (1993) 1837.
- [18] Trager-Cowan C., Sweeney F., Edwards P.R., Wilkinson A.J., Winkelmann A., Day A.P. *et al.* In: Presentation at the annual conference of UK nitrides consortium; 2008.

## Nanomeasurement Systems from Agilent Technologies

Agilent Technologies, the premier measurement company, offers high precision instruments for nanoscience research in academia and industry. Exceptional worldwide support is provided by experienced application scientists and technical service personnel. Agilent's leading-edge R&D laboratories ensure the continued, timely introduction and optimization of innovative, easy-to-use nanomeasurement system technologies.

[www.agilent.com/find/nano](http://www.agilent.com/find/nano)

### Americas

---

Canada	(877) 894 4414
Latin America	305 269 7500
United States	(800) 829 4444

### Asia Pacific

---

Australia	1 800 629 485
China	800 810 0189
Hong Kong	800 938 693
India	1 800 112 929
Japan	0120 (421) 345
Korea	080 769 0800
Malaysia	1 800 888 848
Singapore	1 800 375 8100
Taiwan	0800 047 866
Thailand	1 800 226 008

### Europe & Middle East

---

Austria	43 (0) 1 360 277 1571
Belgium	32 (0) 2 404 93 40
Denmark	45 70 13 15 15
Finland	358 (0) 10 855 2100
France	0825 010 700*
	*0.125 €/minute
Germany	49 (0) 7031 464 6333
Ireland	1890 924 204
Israel	972-3-9288-504/544
Italy	39 02 92 60 8484
Netherlands	31 (0) 20 547 2111
Spain	34 (91) 631 3300
Sweden	0200-88 22 55
Switzerland	0800 80 53 53
United Kingdom	44 (0) 118 9276201

Other European Countries:

[www.agilent.com/find/contactus](http://www.agilent.com/find/contactus)

Product specifications and descriptions in this document subject to change without notice.

© Agilent Technologies, Inc. 2010  
Printed in USA, August 6, 2010  
5990-6349EN